Structures of the Yeast Ribonucleotide Reductase Rnr2 and Rnr4 Homodimers[†,‡]

Monika Sommerhalter,[§] Walter C. Voegtli,[§] Deborah L. Perlstein,[||] Jie Ge,[||] JoAnne Stubbe,[||] and Amy C. Rosenzweig*[,§]

Departments of Biochemistry, Molecular Biology, and Cell Biology and of Chemistry, Northwestern University, Evanston, Illinois 60208, and Departments of Chemistry and of Biology, Massachusetts Institute of Technology, Cambridge, Massachusetts 02139

Received March 11, 2004; Revised Manuscript Received April 21, 2004

ABSTRACT: Class I ribonucleotide reductases (RNRs) catalyze the reduction of ribonucleotides to deoxyribonucleotides. Eukaryotic RNRs comprise two subunits, the R1 subunit, which contains substrate and allosteric effector binding sites, and the R2 subunit, which houses a catalytically essential diiron-tyrosyl radical cofactor. In *Saccharomyces cerevisiae*, there are two variants of the R2 subunit, called Rnr2 and Rnr4. Rnr4 is unique in that it lacks three iron-binding residues conserved in all other R2s. Nevertheless, Rnr4 is required to activate Rnr2, and the functional species in vivo is believed to be a heterodimeric complex between the two proteins. The crystal structures of the Rnr2 and Rnr4 homodimers have been determined and are compared to that of the heterodimer. The homodimers are very similar to the heterodimer and to mouse R2 in overall fold, but there are several key differences. In the Rnr2 homodimer, one of the iron-binding helices, helix αB, is not well-ordered. In the heterodimer, interactions with a loop region connecting Rnr4 helices αA and α3 stabilize this Rnr2 helix, which donates iron ligand Asp 145. Sequence differences between Rnr2 and Rnr4 prevent the same interactions from occurring in the Rnr2 homodimer. These findings provide a structural rationale for why the heterodimer is the preferred complex in vivo. The active-site region in the Rnr4 homodimer reveals interactions not apparent in the heterodimer, supporting previous conclusions that this subunit does not bind iron. When taken together, these results support a model in which Rnr4 stabilizes Rnr2 for cofactor assembly and activity.

Ribonucleotide reductases (RNRs)[1] catalyze the reduction of ribonucleotides to the corresponding deoxyribonucleotides using free-radical chemistry (*1*). These enzymes are responsible for maintaining proper levels of DNA precursors for replication and repair and therefore play a crucial role in all organisms (*2*). RNRs are divided into three classes based on the nature of the catalytically essential radical. Class I RNRs, found in mammals, plants, yeast, DNA viruses, and *Escherichia coli*, consist of two dimeric subunits called R1 and R2. The R1 subunit contains binding sites for substrate and allosteric effectors, and the R2 subunit houses a diiron-tyrosyl radical cofactor. Regulation of eukaryotic class I RNRs during the cell cycle has been studied extensively (*3*, *4*), but most biophysical studies of class I RNRs have focused on the *E. coli* system (*2*). Because eukaryotic RNRs are targets for anticancer drugs (*5*, *6*), an understanding of their structure and function on the molecular level is highly desirable, especially since the discovery of a human R2 variant regulated by the tumor suppressor p53 (*7*).

An obvious choice for a eukaryotic model system is *Saccharomyces cerevisiae* class I RNR. In yeast, four genes encode the RNR subunits. The *RNR1* and *RNR3* genes encode R1-like subunits, Rnr1 and Rnr3. The Rnr3 subunit is not essential and is induced in response to DNA damage (*8*). The *RNR2* (*9*, *10*) and *RNR4* (*11*, *12*) genes encode the Rnr2 and Rnr4 proteins, which correspond to the R2-like subunits. The Rnr4 protein is unique in that it lacks 6 of 16 residues conserved in nearly all R2s, including three residues involved in coordinating iron. As a result, Rnr4 cannot accommodate a diiron center. Nevertheless, Rnr4 deletion is lethal in some yeast strains and impairs cell growth in others (*11*, *12*). Initial insight into the possible function of Rnr4 came from studies showing that Rnr4 is required to assemble the diiron-tyrosyl radical cofactor in Rnr2 and that Rnr4 forms a heterodimeric complex with Rnr2 (*13*−*15*). On the basis of these data, it was proposed that Rnr4 functions either as a metallochaperone, inserting iron into Rnr2 (*13*), or as a molecular chaperone, directing Rnr2 folding (*14*). However, Rnr4 does not bind iron, ruling out a metallochaperone function (*15*, *16*). In addition, Rnr2 folds independently of Rnr4 (*15*) and can be crystallographically characterized (vide infra). A role in global folding is therefore unlikely, but Rnr4 could still serve as a local folding aid, holding Rnr2 in an appropriate conformation to receive iron from another source.

[†] This work was supported by NIH Grants GM58518 (to A.C.R.) and GM29595 (to J.S.). W.C.V. was supported in part by NIH training Grant GM08382, and D.L.P. was supported in part by NIH training Grant 5T32 CA 09112-28.

[‡] Coordinates have been deposited in the Protein Data Bank with accession codes 1SMQ for the Rnr2 homodimer and 1SMS for the Rnr4 homodimer.

* To whom correspondence should be addressed. Telephone: (847) 467-5301. Fax: (847) 467-6489. E-mail: amyr@northwestern.edu.

[§] Northwestern University.

[||] Massachusetts Institute of Technology.

[1] Abbreviations: RNR, ribonucleotide reductase; Rnr2, yeast ribonucleotide reductase Rnr2 protein; Rnr4, yeast ribonucleotide reductase Rnr4 protein; PEG, polyethylene glycol; EMTS, ethylmercurithiosalicylate; rms, root mean square.

10.1021/bi049510m CCC: $27.50
Published on Web 05/26/2004

If Rnr4 is a local folding chaperone, it could either dissociate from Rnr2 after the cofactor is inserted or remain associated for activity. Several lines of evidence suggest that the active form of yeast Rnr2 in vivo is the heterodimeric complex between Rnr2 and Rnr4. First, the heterodimer contains 0.6−0.8 tyrosyl radicals, a value comparable to that observed for other R2 homodimers and suggestive of a conserved half-site reactivity in all R2s (*15*). Second, Rnr2 and Rnr4 are present in comparable concentrations in vivo (*15*). Third, Rnr2 and Rnr4 colocalize during the normal cell cycle and redistribute similarly in response to genotoxic stress (*17*). Understanding why yeast R2, unlike all other R2s studied thus far, exists as a heterodimer is critical to further use of yeast RNR as a model system. To elucidate why the heterodimer might be the preferred complex in vivo, we have determined the crystal structures of the Rnr2 and Rnr4 homodimers. A detailed comparison with the previously determined structure of the heterodimer (*16*) reveals subtle yet significant differences that provide new insight into the relative stabilities of the different species.

EXPERIMENTAL PROCEDURES

Crystallization. Rnr4 and $(His)_6$-tagged Rnr2 were purified as described previously (*15*). Purified $(His)_6$−Rnr2 was diluted with 50 mM Tris at pH 7.5 to a final concentration of 3 mg/mL. Crystals were obtained at 14 °C by using the hanging-drop technique. Drops consisting of 1 μL of protein solution and 1 μL of precipitant solution were equilibrated versus 750 μL of precipitant solution composed of 100 mM succinate at pH 4.8, 15% (w/v) polyethylene glycol (PEG) 3350, and 200 mM lithium acetate. Long rectangular crystals of maximum dimensions 0.1 × 0.1 × 1.0 mm appeared within 2−4 days. Crystals for data collection were transferred to a cryosolution composed of the precipitant solution with 20% (v/v) ethylene glycol and flash-cooled in liquid nitrogen after 1−2 min.

Purified Rnr4 for crystallization was diluted to 10 mg/mL in 50 mM Tris at pH 7.5. Crystals were obtained at room temperature by using the hanging-drop method. Drops containing 3 μL of protein solution and 3 μL of precipitant solution were suspended on the lid of a completely sealed Petri dish containing 3 mL of precipitant solution. The precipitant solution consisted of 50 mM HEPES at pH 7.5, 26% (w/v) PEG 1000, 5% (v/v) ethanol, 200 mM NaCl, and 1 mM ethylmercurithiosalicylate (EMTS). Large, fragile crystals (0.2 × 0.2 × 1.5 mm) grew in the shape of hexagonal rods within 3 days. Crystals for data collection were prepared by layering a small amount of cryosolution, comprising the precipitant plus an additional 20% (v/v) ethylene glycol, over the crystallization drop. Large, single crystals were quickly passed through the cryosolvent layer using a rayon loop and immediately flash-cooled in liquid nitrogen.

Data Collection and Structure Determination. Diffraction data (Table 1) were collected at the DuPont−Northwestern−Dow Collaborative Access Team (DND-CAT) beamline at the Advanced Photon Source at −160 °C and a wavelength of 1.00 Å using a 2K × 2K Mar CCD detector. The Rnr2 crystals belong to the space group $P1$ with unit cell dimensions: $a = 79.7$ Å, $b = 79.6$ Å, $c = 88.1$ Å, $\alpha = 83.5°$, $\beta = 83.5°$, and $\gamma = 70.8°$. The Rnr4 crystals belong to the space group $P6_1$ with unit cell dimensions: $a = b = 79.6$ Å, and $c = 218.1$ Å. The Rnr2 data were processed with MOSFLM (*18*) and SCALA (*19*), and the Rnr4 data were processed with DENZO and SCALEPACK (*20*).

Table 1: Data Collection and Refinement Statistics

	Rnr2	Rnr4
Data Collection		
resolution range (Å)	87−3.10	12−3.10
unique observations	35 134	13 332
total observations	168 766	239 131
completeness (%)	94.6 (96.0)	93.6 (94.1)
R_{sym}[a]	0.059 (0.294)	0.088 (0.424)
$<I/\sigma>$	7.2 (2.5)	13.4 (2.4)
Refinement		
resolution range (Å)	25−3.10	12−3.10
number of reflections	34 663	12 869
R factor[b]	0.272	0.266
R free	0.303	0.305
number of protein, nonhydrogen atoms	10 694	5182
number of nonprotein atoms	0	4
rms bond length (Å)	0.010	0.008
rms bond angles (deg)	1.6	1.4
average *B* values (Å^2)		
main chain	68.4	71.2
side chain	71.5	71.7

[a] $R_{sym} = \Sigma|I_{obs} - I_{avg}|/\Sigma I_{obs}$, where the summation is over all reflections. Values in parentheses are for the highest resolution shells, 3.27−3.10 Å for Rnr2 and 3.15−3.10 Å for Rnr4. [b] *R* factor $= \Sigma|F_{obs} - F_{calc}|/\Sigma F_{obs}$. For calculation of *R* free, 9 and 5% of the reflections were reserved for Rnr2 and Rnr4, respectively.

The structures of the Rnr2 and Rnr4 homodimers were solved by molecular replacement with AMoRe (*19*) and CNS (*21*) using a monomer of Rnr2 or Rnr4 from the heterodimer structure (*16*) as a starting model. Both models were refined by iterative cycles of X-ray weight optimization, rigid-body refinement, restrained individual *B* factor refinement, energy minimization, and low-temperature torsional simulated annealing in CNS (*21*). Noncrystallographic symmetry restraints were used throughout the refinements. Adjustments to the models were performed in XtalView (*22*) and O (*23*) using composite omit $2F_o - F_c$ electron density maps. The progress of the refinement was monitored by the free *R* value. The Rnr2 model consists of two homodimers. One monomer in each of the two dimers includes residues 26−144 and 150−359, and the second monomer includes residues 26−57, 69−144, and 150−359. No electron density was visible for residues 145−149 in all four monomers. The final Rnr4 model consists of one homodimer with residues 3−305 and 315−325 for each monomer. In addition, four strong peaks ($>11\sigma$) in difference Fourier maps were modeled as mercury ions derived from EMTS. Ramachandran plots generated with PROCHECK (*24*) indicate that the models exhibit good geometry with 99.7% of the Rnr2 residues and 98.3% of the Rnr4 residues in the most favored and additionally allowed regions. Accessible surface-area calculations were performed with the CCP4 program AREAIMOL (*19*) or with CNS (*21*) using a molecular probe of radius 1.4 Å. Residues involved in crystal-packing contacts and the dimer interfaces were identified with the CCP4 program CONTACT (*19*) or CNS (*21*). Figures were generated with MOLSCRIPT (*25*) and RASTER3D (*26*).

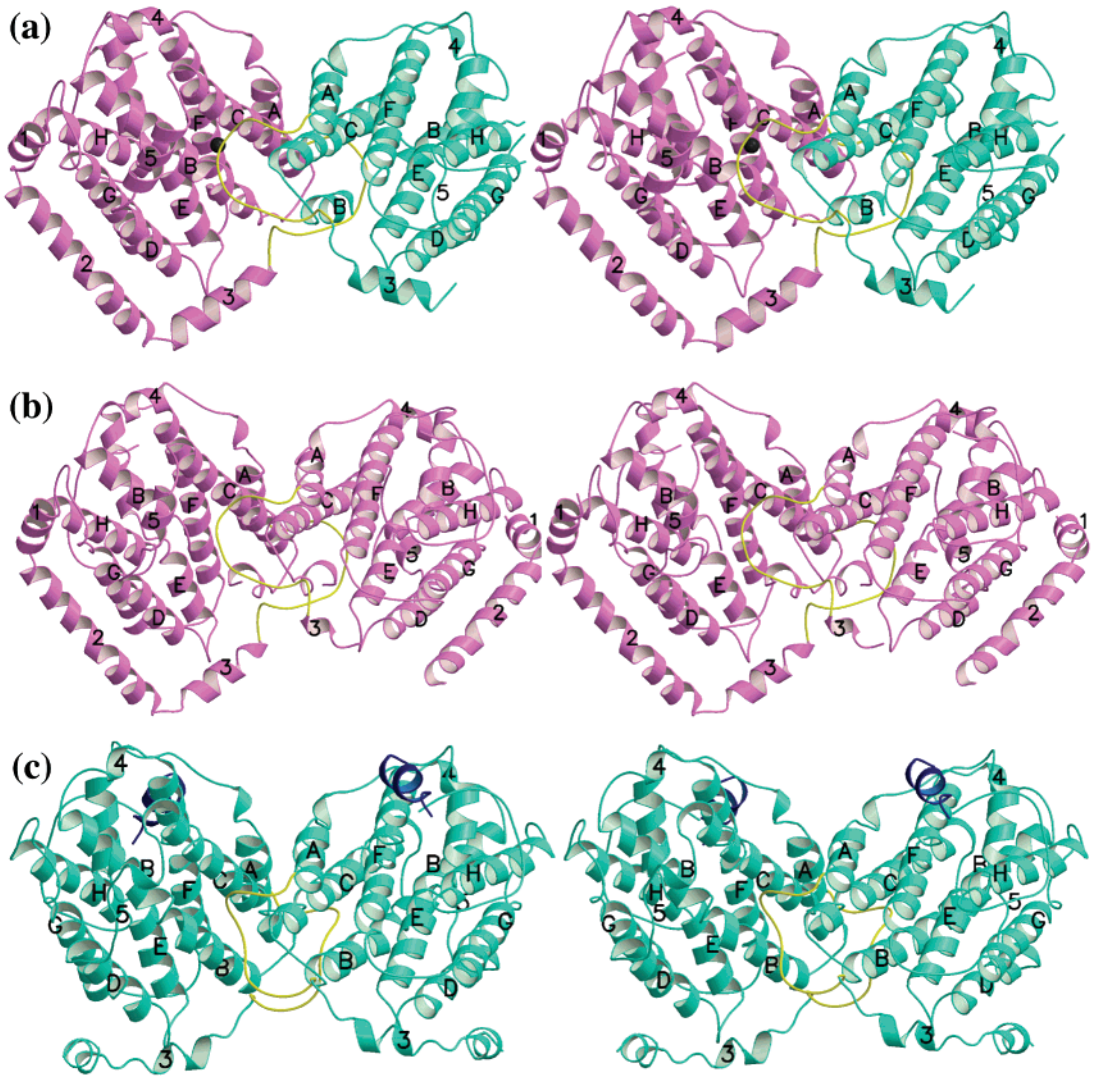

FIGURE 1: Stereoviews of (a) the heterodimeric complex (PDB accession code 1JK0) between Rnr2 (pink) and Rnr4 (green), (b) the Rnr2 homodimer, and (c) the Rnr4 homodimer. The flexible loop connecting helices α3 and αA is shown in yellow. For the Rnr4 homodimer, the C-terminal helix spanning residues 315−325 is shown in blue.

RESULTS AND DISCUSSION

Rnr2 Homodimer. The overall fold of the Rnr2 monomer is very similar to its fold in the heterodimeric complex (parts a and b of Figure 1). The eight longest helices (αA−αH) form an α-helical bundle like those in *E. coli* (*27*) and mouse R2 (*28*). Two smaller helices, α4 and α5, cap the eight helix bundle. The Rnr2 model contains three additional N-terminal helices (α1−α3) encompassing residues 26−70. This part of the sequence was also observed in the heterodimer but not in the crystal structure of mouse R2. In the heterodimer structure, the presence of an ordered N terminus in Rnr2 was attributed to participation of the three helices in crystal-packing interactions (*16*). In the Rnr2 homodimer, the N terminus of one monomer is involved in crystal contacts, but the N terminus of the second monomer is exposed to a solvent channel. As a result, residues 58−68 are not visible in the second monomer. The N terminus of Rnr2 and mammalian R2 subunits is more extended than that in Rnr4, plant, or *E. coli* systems. In mice, part of this sequence is important for R2 protein degradation during mitosis (*29*). The C-terminal 40 residues of Rnr2, which were not observed in the heterodimer structure, are also not visible in the homodimer structure. These residues are crucial for interaction with the R1 subunit (*14*, *30*, *31*). For the mouse and *E. coli* proteins, the C termini only become structured upon complex formation between the two subunits (*32*, *33*).

The Rnr2 monomer from the homodimer can be superimposed on that from the heterodimer with an rms deviation of 0.42 Å for 329 Cα coordinates. There are no significant structural changes (Figure 2). The only major difference between Rnr2 in the homodimer and in the heterodimer is more disorder in helix αB. For the Rnr2 homodimer, this region has high *B* values and residues 145−149 could not be modeled. This helix αB is not only part of the central core of the eight helix bundle but also provides one of the ligands, Asp 145, to the diiron center. Aside from the absence of Asp 145, all of the other ligands provided to the diiron center occupy the same positions as in the heterodimer structure. In the heterodimer, strong electron density in the Rnr2 active site was modeled as a single Zn^{II} ion based on anomalous difference Fourier maps calculated at different wavelengths (*16*). In contrast, no significant extra electron density is observed in the Rnr2 homodimer active site.

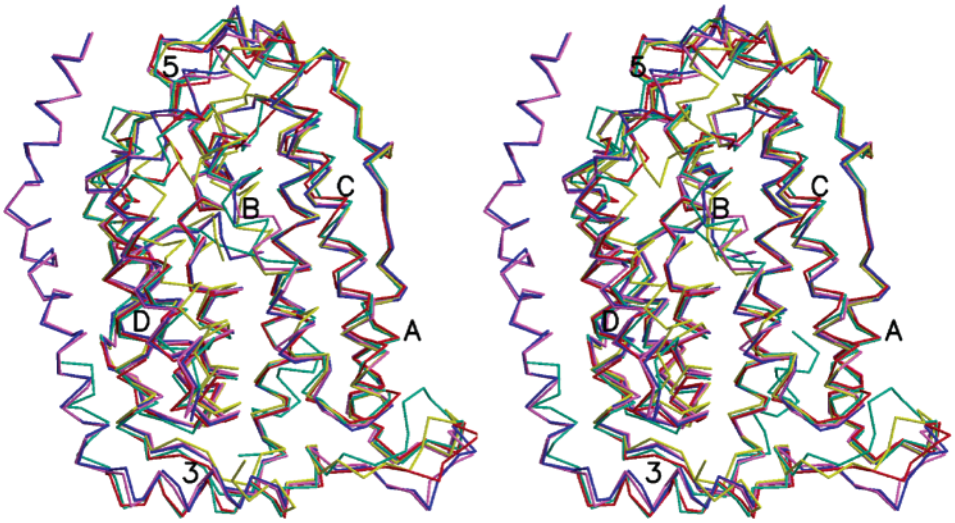

FIGURE 2: Stereo superposition of Rnr2 in the homodimer (magenta), Rnr2 in the heterodimer (blue, PDB accession code 1JK0), Rnr4 in the homodimer (green), Rnr4 in the heterodimer (red, PDB accession code 1JK0), and mouse R2 (yellow, PDB accession code 1XSM).

Rnr4 Homodimer. The fold of the Rnr4 monomer is very similar to that observed in the heterodimer with a core of eight α helices (parts a and c of Figure 1). In Rnr4, the helical character of the region corresponding to α5 is disrupted by Pro 146. For the homodimer, the visible part of the N-terminal sequence begins at residue 3 as compared to 11 for Rnr4 in the heterodimer. These additional residues comprise a short α helix that points in a different direction than the analogous α2 in Rnr2. Notably, the Rnr4 model includes 20 additional residues (296−305 and 315−325) at the C terminus not observed in the heterodimer (Figure 1c). The presence of a helix comprising residues 315−325 is especially surprising. This helix is not connected to the C terminus but could be traced clearly in the electron density map based on the presence of two aromatic residues, Phe 316 and Tyr 323. Four residues derived from this helix are involved in key crystal-packing interactions, explaining why this sequence, which is expected to be ordered only in the presence of the Rnr1 subunit, is visible. These residues in the Rnr4 homodimer structure provide the first glimpse of the C terminus of any R2 subunit.

The Rnr4 monomers from the homodimer and the heterodimer can be superimposed with an rms deviation of 0.87 Å for 257 Cα coordinates. Although the overall fold of Rnr4 remains the same, the loop connecting helices α3 and αA has adopted a different conformation, shifting toward the loop between helices αB and αC (Figure 2). This shift is likely due to the presence of the ordered helix comprising residues 315−325. In both halves of the Rnr4 monomer, this loop packs against residues 315−325 from symmetry-related molecules, preventing it from assuming the conformation observed in the heterodimer. The largest shift in the loop is observed at residues Arg 34 and Phe 35, of which the Cα atoms move ∼8.5 Å relative to their positions in the heterodimer. As a result, Phe 35 occupies different pockets in the two structures. In the Rnr4 homodimer, the side chain of Phe 35 is packed against the phenol group of Tyr 99 and the alkane side chain of Lys 98 from the second monomer. The amino group of Lys 98 is within hydrogen-bonding distance of Ser 128 from the same monomer, further stabilizing this arrangement. In the heterodimer, Phe 35 stacks against the side chain of Rnr2 Phe 201, located in a region structurally distinct from that analogous to Rnr4 residues 98−99. Rnr4 Arg 34 also occupies different positions in the two structures. In the homodimer, Arg 34 interacts with Glu 102 from the second monomer, whereas in the heterodimer, Arg 34 does not participate in the dimer interface but, instead, forms a salt bridge with Glu 112 from the same monomer.

Another important difference between the Rnr4 homodimer and Rnr4 in the heterodimeric complex is that residues 91−99 from helix αB, which could not be modeled in the heterodimer, are visible, most likely because of the interaction with Phe 35 from the opposite monomer. These residues correspond to the disordered region encompassing residues 145−149 in the Rnr2 homodimer and include Asp 93, the equivalent of the iron ligand Asp 145 in Rnr2. Unexpectedly, the side chain of Asp 93 is not located within the "active site" region of Rnr4 (Figure 3). Instead, Asn 94 points into the active site and forms a hydrogen bond with Ser 128. Similar to the heterodimer structure, Arg 220 interacts with Glu 124, but an additional hydrogen bond between Glu 124 and Asn 97 is also observed. A water molecule present in the heterodimer was not modeled in this structure because of the low resolution. This arrangement of residues in the Rnr4 active-site region supports previous conclusions that Rnr4 does not bind iron (*15*, *16*).

Dimer Interfaces. The dimer interfaces in the two homodimers and the heterodimer are similar in size, with buried surface areas of 2517 (1223 Å^2 for Rnr2 and 1294 Å^2 for Rnr4), 2339, and 2462 Å^2 for the heterodimer, the Rnr2 homodimer, and the Rnr4 homodimer, respectively. These values are comparable to the 2967 Å^2 buried surface area in mouse R2. The interface comprises residues located primarily on helices αA and αC and is capped by the loop connecting αA and α3. On each side of the interface, this loop extends over the other monomer (Figure 1). Both hydrophobic and hydrophilic residues participate in key interactions at the interface. In Rnr2, residues Phe 107, Phe 171, and Met 174 form a central hydrophobic patch. The equivalent residues in Rnr4 are Phe 56, Phe 119, and Met 122. This hydrophobic patch is flanked by salt bridges. In Rnr2, the side chain of Lys 101 from one monomer is hydrogen-bonded to the side chains of Glu 111 and Glu 181 from the second monomer

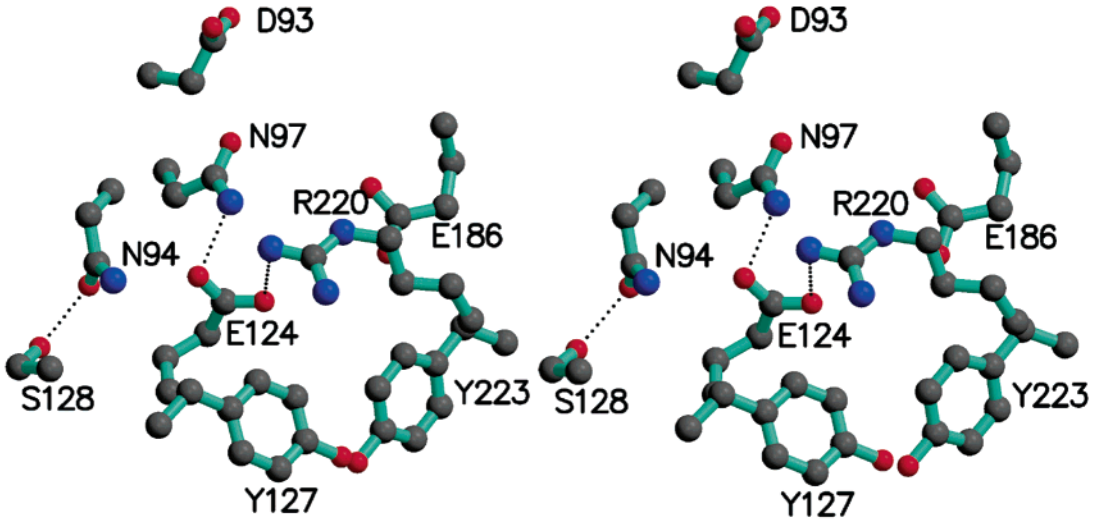

FIGURE 3: Stereoview of the Rnr4 active-site region.

(a)

Rnr2 *Saccharomyces cerevisiae*	84	E	R	T	V	L	F	P	90
Rnr4 *Saccharomyces cerevisiae*	33	R	R	F	V	M	F	P	39
Rnr2 *Schizosaccharomyces pombe*	74	H	R	F	V	L	F	P	80
Rnr2 *Mus musculus*	79	R	R	F	V	V	F	P	85
Rnr2 *Homo sapiens*	78	R	R	F	V	I	F	P	84
Rnr2 *Brachydanio rerio*	75	H	R	F	V	I	F	P	81
Rnr2 *Drosophila melanogaster*	82	R	R	F	V	I	F	P	88
Rnr2 *Caenorhabditis elegans*	70	N	R	F	V	I	F	P	76

(b)

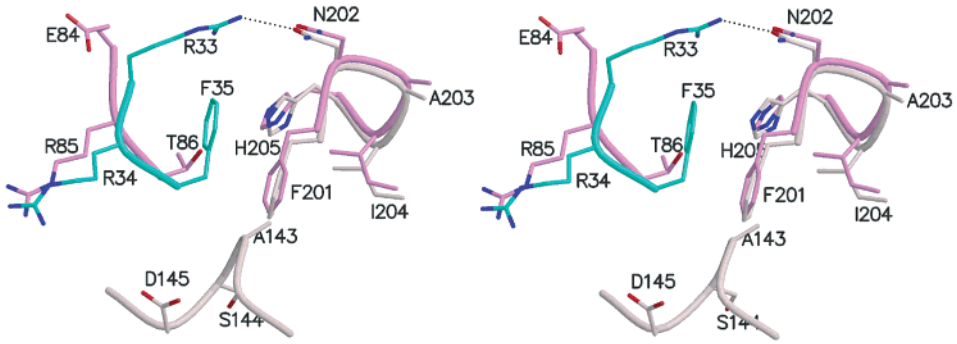

FIGURE 4: Dimer interface residues derived from the loop region connecting α3 and αA. (a) Sequence alignment of loop residues. Swiss-Prot accession codes: *S. cerevisiae* Rnr2, RIR2_YEAST; *S. cerevisiae* Rnr4, RIR4_YEAST; *S. pombe* Rnr2, RIR2_SCHPO; *Mus musculus* Rnr2, RIR2_MOUSE; *Homo sapiens* Rnr2, RIR2_HUMAN; *Brachydanio rerio* Rnr2, RIR2_BRARE; *Drosophila melanogaster* Rnr2, RIR2_DROME; *Caenorhabditis elegans* Rnr2, RIR2_CAEEL. (b) Stereoview of dimer interface interactions involving these residues and the nearby segment of helix αB including iron ligand Asp 145. The Rnr2 homodimer is shown in pink, and the heterodimer is shown in green (Rnr4) and light pink (Rnr2).

and vice versa. Similarly, Rnr4 Lys 50 interacts with Rnr4 Glu 60 and Glu 129. In the Rnr2 homodimer, an additional close contact is observed between the two Val 153 residues, housed on helix αB.

The conservation of these interactions among the two homodimers and the heterodimer indicates that the individual monomers are well-suited to form different dimer combinations. The core interface is the same regardless of which monomers are present. Nevertheless, the tyrosyl radical content, quantitative Western blotting (*15*), and subcellular localization patterns (*17*) indicate that the heterodimer is the active species in vivo. Furthermore, several empirical observations imply that the heterodimer may be the more stable species. First, soluble, folded Rnr2 cannot be obtained without a $(His)_6$ tag (*13*, *14*). Second, the heterodimer can be selectively crystallized from a mixture of purified Rnr2 and Rnr4 homodimers (*16*). How are varying stabilities conferred in the context of such similar dimer interfaces? The capping loop region connecting α3 and αA provides part of the answer. In contrast to the interactions in the central interface region, interactions involving this loop are not completely conserved.

In particular, Phe 35 in Rnr4 is replaced with a threonine, Thr 86, in Rnr2 (Figure 4a). In the heterodimer, Phe 35 from Rnr4 extends into a pocket lined by Rnr2 Phe 201 and Rnr2 His 205 from helix α5, stacking nicely with Phe 201. The same interaction cannot be formed by Rnr2 Thr 86 in the Rnr2 homodimer (Figure 4b). Notably, only Rnr2 has a

threonine at this position, whereas most other organisms contain a conserved phenylalanine residue (Figure 4a). Several other *Saccharomyces* species, including *S. castellii*, *S. mikatae*, *S. bayanus*, and *S. kudriavzevii*, contain either a threonine, serine, or histidine at this position (*34*). All of these species also have a gene encoding an Rnr4-like protein. The potential significance of this substitution in Rnr2 is underscored by the observation that the one *Saccharomyces* species, *S. kluyveri*, that does contain a phenylalanine at this position in Rnr2 does not appear to have a protein corresponding to Rnr4. Moreover, other fungi that only have an Rnr2-like protein, including *Schizosaccharomyces pombe*, *Kluyveromyces waltii*, and *Ashbya gossypii*, also contain a phenylalanine at this position.

Another difference involving the loop connecting α3 and αA involves Rnr4 Arg 33. In the heterodimer, this residue is hydrogen-bonded to the side chain of Rnr2 Asn 202. The Rnr2 residue analogous to Rnr4 Arg 33 is Glu 84. In the Rnr2 homodimer, the shorter side chain of Glu 84 does not interact with residues on the other monomer but instead points toward the solvent (Figure 4b). In contrast, the second arginine in the loop sequence is well-conserved (Rnr2 Arg 85 and Rnr4 Arg 34). In the Rnr2 homodimer and in the heterodimer, it forms an intramonomer hydrogen bond with a glutamic acid residue at the beginning of helix αC (Rnr2 Glu 164 and Rnr4 Glu 112). In the Rnr4 homodimer, Arg 34 from one monomer interacts with Glu 102 from the second monomer. When taken together, these interactions result in helix αB, which houses the iron ligand Asp 145, being more exposed in the Rnr2 homodimer than in the heterodimer (Figure 4b), and explain why residues 145−149 are disordered in the homodimer. The heterodimer might therefore be preferred in vivo because helix αB is held in the appropriate conformation to form and stabilize the diiron center.

Comparison to Mouse R2. The structures of the Rnr2 and Rnr4 monomers from the two homodimers are very similar to that of the mouse R2 monomer, with rms deviations of 1.00 Å for 250 Rnr2 Cα coordinates and 1.24 Å for 247 Rnr4 Cα coordinates. The most significant difference is the position of Rnr2 helices αD and α5 and the corresponding Rnr4 helices (Figure 2). As noted previously (*16*), these helices in Rnr2 are shifted by ∼5 Å away from the four-helix bundle that houses the diiron center, rendering the active site even more accessible than that in mouse R2 (*28*). In mouse R2, the loop region connecting α3 and αA adopts a conformation intermediate between those observed in the Rnr4 and Rnr2 homodimer structures (Figure 2). Residue Phe 81 from this loop (Phe 35 in Rnr4, Figure 4a) is located in a pocket lined by the alkane side chains of Asn 143 and Glu 144 and the Cα atom of Gly 140 from the second monomer. These residues, which are proximal to iron ligand Asp 139, are derived from the part of helix αB that is poorly defined in the Rnr2 homodimer (residues 143−151). Analogous to the heterodimer, interactions involving Phe 81 likely stabilize this helix. Like the heterodimer and the Rnr2 homodimer, the preceding residue Arg 80 (Figure 4a) forms a hydrogen bond with Glu 158 from the same monomer.

Another notable difference between mouse R2 and yeast Rnr2 is the conformation of the aspartic acid residue in the active site. In Rnr2, this residue, Asp 145, is either not visible (homodimer) or points away from the iron-binding site (heterodimer). The equivalent residue in mouse R2, Asp 139, was modeled pointing toward the diiron center, although the iron-binding site closer to this residue and to the tyrosyl radical site was not occupied (*28*). Interestingly, these different positions of the active-site aspartic acid are all observed at relatively low pH values (mouse R2, pH 4.7; Rnr2 homdimer, pH 4.8; and heterodimer, pH 5.3). It may be that a higher pH value would affect the position of this residue in the yeast system. Raising the pH of mouse R2 crystals from pH 4.8 to 6.0 allowed loading of two, rather than one, cobalt ions, suggesting that pH can affect the metal center in mouse R2 (*35*). However, recent studies of diferrous *E. coli* R2 suggest that pH does not significantly affect the coordination geometry (*36*).

Conclusions. In summary, the Rnr2 and Rnr4 monomers in the homodimeric and heterodimeric complexes are very similar in their overall fold to one another and to mouse R2. In the Rnr2 homodimer, helix αB, which provides iron ligand Asp 145, is notably less-ordered than in the heterodimer. The ordering of this helix in the heterodimer can be attributed to interactions with the loop connecting Rnr4 helices αA and α3, which adopts a considerably different conformation than in the Rnr4 homodimer. In particular, the interaction of this loop with Rnr2 compensates for the presence of a threonine residue, Thr 86, in a position occupied by a phenylalanine in other eukaryotic R2s. In contrast, other interactions at the dimer interfaces are highly conserved among the two homodimers and the heterodimer. The current data therefore suggest that the role of Rnr4 is to stabilize helix αB and provide a structural rationale for the heterodimer being the active species in vivo. It is likely that Rnr4 stabilizes Rnr2 both for assembly of the diiron center, perhaps by facilitating interactions with yet to be identified metal-delivery factors, and for subsequent enzyme activity. Why yeast RNR has evolved to function optimally with only one diiron-tyrosyl radical cofactor per dimer remains unclear but supports the notion that half-site reactivity is a general feature of radical-containing enzymes (*1*).

ACKNOWLEDGMENT

We thank J. Pham for assistance with Rnr4 crystallization.

REFERENCES

1. Stubbe, J., and Donk, W. A. v. d. (1998) Protein radicals in enzyme catalysis, *Chem. Rev. 98*, 705−762.
2. Eklund, H., Uhlin, U., Färnegårdh, M., Logan, D. T., and Nordlund, P. (2001) Structure and function of the radical enzyme ribonucleotide reductase, *Prog. Biophys. Mol. Biol. 77*, 177−268.
3. Chabes, A., and Thelander, L. (2000) Controlled protein degradation regulates ribonucleotide reductase activity in proliferating mammalian cells during normal cell cycle and in response to DNA damage and replication blocks, *J. Biol. Chem. 275*, 17747−17753.
4. Elledge, S. J., Zheng, Z., and Allen, J. B. (1992) Ribonucleotide reductase: Regulation, regulation, regulation, *Trends Biochem. Sci. 17*, 119−123.
5. Heinemann, V. (2001) Gemcitabine: Progress in the treatment of pancreatic cancer, *Oncology 60*, 8−18.
6. Gwilt, P. R., and Tracewell, W. G. (1998) Pharmacokinetics and pharmacodynamics of hydroxyurea, *Clin. Pharmocokinet. 35*, 347−358.
7. Tanaka, H., Arakawa, H., Yamaguchi, T., Shiraishi, K., Fukuda, S., Matsui, K., Takei, Y., and Nakamura, Y. (2000) A ribonucleotide reductase gene involved in a p53-dependent cell-cycle checkpoint for DNA damage, *Nature 404*, 42−49.
8. Elledge, S. J., and Davis, R. W. (1990) Two genes differentially regulated in the cell cycle and by DNA-damaging agents encode

alternative regulatory subunits of ribonucleotide reductase, *Genes Dev. 4*, 740−751.
9. Elledge, S. J., and Davis, R. W. (1987) Identification and isolation of the gene encoding the small subunit of ribonucleotide reductase from *Saccharomyces cerevisiae*: DNA damage-inducible gene required for mitotic viability, *Mol. Cell. Biol. 7*, 2783−2793.
10. Hurd, H. K., Roberts, C. W., and Roberts, J. W. (1987) Identification of the gene for the yeast ribonucleotide reductase small subunit and its inducibility by methyl methanesulfonate, *Mol. Cell. Biol. 7*, 3673−3677.
11. Huang, M., and Elledge, S. J. (1997) Identification of *RNR4*, encoding a second essential small subunit of ribonucleotide reductase in *Saccharomyces cerevisiae*, *Mol. Cell. Biol. 17*, 6105−6113.
12. Wang, P. J., Chabes, A., Casagrande, R., Tian, X. C., Thelander, L., and Huffaker, T. C. (1997) Rnr4p, a novel ribonucleotide reductase small-subunit protein, *Mol. Cell. Biol. 17*, 6114−6121.
13. Nguyen, H.-H. T., Ge, J., Perlstein, D. L., and Stubbe, J. (1999) Purification of ribonucleotide reductase subunits Y1, Y2, Y3, and Y4 from yeast: Y4 plays a key role in diiron cluster assembly, *Proc. Natl. Acad. Sci., U.S.A. 96*, 12339−12344.
14. Chabes, A., Domkin, V., Larsson, G., Liu, A., Gräslund, A., Wijmenga, S., and Thelander, L. (2000) Yeast ribonucleotide reductase has a heterodimeric iron-radical-containing subunit, *Proc. Natl. Acad. Sci. U.S.A. 97*, 2474−2479.
15. Ge, J., Perlstein, D. L., Nguyen, H. H., Bar, G., Griffin, R. G., and Stubbe, J. (2001) Why multiple subunits (Y2 and Y4) for yeast ribonucleotide reductase? Toward understanding the role of Y4, *Proc. Natl. Acad. Sci. U.S.A. 98*, 10067−10072.
16. Voegtli, W. C., Ge, J., Perlstein, D. L., Stubbe, J., and Rosenzweig, A. C. (2001) Structure of the yeast ribonucleotide reductase Y2Y4 heterodimer, *Proc. Natl. Acad. Sci. U.S.A. 98*, 10073−10078.
17. Yao, R., Zhang, Z., An, X., Bucci, B., Perlstein, D. L., Stubbe, J., and Huang, M. (2003) Subcellular localization of yeast ribonucleotide reductase regulated by the DNA replication and damage checkpoint pathways, *Proc. Natl. Acad. Sci. U.S.A. 100*, 6628−6633.
18. Powell, H. R. (1999) The Rossmann Fourier autoindexing algorithm in MOSFLM, *Acta Crystallogr., Sect. D 55*, 1690−1695.
19. Collaborative Computational Project Number 4 (1994) The CCP4 suite programs for protein crystallography, *Acta Crystallogr., Sect. D 50*, 760−763.
20. Otwinowski, Z., and Minor, W. (1997) Processing of X-ray diffraction data collected in oscillation mode, *Methods Enzymol. 276*, 307−326.
21. Brünger, A. T., Adams, P. D., Clore, G. M., DeLano, W. L., Gros, P., Grosse-Kunstleve, R. W., Jiang, J.-S., Kuszewski, J., Nilges, M., Pannu, N. S., Read, R. J., Rice, L. M., Simonson, T., and Warren, G. L. (1998) Crystallography and NMR System: A new software suite for macromolecular crystallography, *Acta Crystallogr., Sect. D 54*, 905−921.
22. McRee, D. E. (1999) XtalView Xfit−A versatile program for manipulating atomic coordinates and electron density, *J. Struct. Biol. 125*, 156−165.
23. Jones, T. A., Zou, J.-Y., Cowan, S. W., and Kjeldgaard, M. (1991) Improved methods for building protein models in electron density maps and location of errors in these models, *Acta Crystallogr., Sect. A 47*, 110−119.
24. Laskowski, R. A. (1993) PROCHECK: A program to check the stereochemical quality of protein structures, *J. Appl. Crystallogr. 26*, 283−291.
25. Kraulis, P. J. (1991) MOLSCRIPT: A program to produce detailed and schematic plots of protein structures, *J. Appl. Crystallogr. 24*, 946−950.
26. Merritt, E. A., and Bacon, D. J. (1997) Raster3D: Photorealistic molecular graphics, *Methods Enzymol. 277*, 505−524.
27. Nordlund, P., and Eklund, H. (1993) Structure and function of the *Escherichia coli* ribonucleotide reductase protein R2, *J. Mol. Biol. 231*, 123−164.
28. Kauppi, B., Nielsen, B. B., Ramaswamy, S., Larsen, I. K., Thelander, M., Thelander, L., and Eklund, H. (1996) The three-dimensional structure of mammalian ribonucleotide reductase protein R2 reveals a more-accessible iron-radical site than *Escherchia coli* R2, *J. Mol. Biol. 262*, 706−720.
29. Chabes, A. L., Pfleger, C. M., Kirschner, M. W., and Thelander, L. (2003) Mouse ribonucleotide reductase R2 protein: A new target for anaphase-promoting complex-Cdh1-mediated proteolysis, *Proc. Natl. Acad. Sci. U.S.A. 100*, 3925−3929.
30. Climent, I., Sjöberg, B.-M., and Huang, C. Y. (1992) Site-directed mutagenesis and deletion of the carboxyl terminus of *Escherichia coli* ribonucleotide reductase protein R2. Effects on catalytic activity and subunit interaction, *Biochemistry 31*, 4801−4807.
31. Fisher, A., Yang, F. D., Rubin, H., and Cooperman, B. S. (1993) R2 C-terminal peptide inhibition of mammalian and yeast ribonucleotide reductase, *J. Med. Chem. 36*, 3859−3862.
32. Lycksell, P. O., Ingemarson, R., Davis, R., Gräslund, A., and Thelander, L. (1994) H^1 NMR studies of mouse ribonucleotide reductase−The R2 protein carboxyl-terminal tail, essential for subunit interaction, is highly flexible but becomes rigid in the presence of protein R1, *Biochemistry 33*, 2838−2842.
33. Lycksell, P. O., and Sahlin, M. (1995) Demonstration of segmental mobility in the functionally essential carboxyl-terminal part of ribonucleotide reductase protein R2 from *Escherichia coli*, *FEBS Lett. 368*, 441−444.
34. Dolinski, K., Balakrishnan, R., Christie, K. R., Costanzo, M. C., Dwight, S. S., Engel, S. R., Fisk, D. G., Hirschman, J. E., Hong, E. L., Issel-Tarver, L., Sethuraman, A., Theesfeld, C. L., Binkley, G., Lane, C., Schroeder, M., Dong, S., Weng, S., Andrada, R., Botstein, D., and Cherry, J. M., *Saccharomyces* Genome Database, http://www.yeastgenome.org/.
35. Strand, K. R., Karlsen, S., and Andersson, K. K. (2002) Cobalt substitution of mouse R2 ribonucleotide reductase as a model for the reactive diferrous state, *J. Biol. Chem. 277*, 34229−34238.
36. Voegtli, W. C., Sommerhalter, M., Saleh, L., Baldwin, J., Bollinger, J. M., Jr., and Rosenzweig, A. C. (2003) Variable coordination geometries at the diiron(II) active site of ribonucleotide reductase R2, *J. Am. Chem. Soc. 125*, 15822−15830.

BI049510M